J Arid Land (2023) 15(12): 1490–1509
https://doi.org/10.1007/s40333-023-0112-6

Science Press Springer-Verlag

Integrating stable isotopes and factor analysis to delineate the groundwater provenance and pollution sources in the northwestern part of the Amman-Al Zarqa Basin, Jordan

Mutawakil OBEIDAT[1*], Ahmad AL-AJLOUNI[2], Eman BANI-KHALED[2], Muheeb AWAWDEH[3], Muna ABU-DALO[2]

[1] Basic Sciences and Humanities Department, Faculty of Science and Arts, Water Diplomacy Centre, Jordan University of Science and Technology, Irbid 22110, Jordan;
[2] Chemistry Department, Jordan University of Science and Technology, Irbid 22110, Jordan;
[3] Laboratory of Applied Geoinformatics, Department of Earth and Environmental Sciences, Yarmouk University, Irbid 21163, Jordan

Abstract: Globally, groundwater contamination by nitrate is one of the most widespread environmental problems, particularly in arid and semiarid areas, which are characterized by low amounts of rainfall and groundwater recharge. The stable isotope composition of groundwater (δ^2H-H_2O and δ^{18}O-H_2O) and dissolved nitrate (δ^{15}N-NO_3^- and δ^{18}O-NO_3^-) and factor analysis (FA) were applied to explore groundwater provenance, pollution, and chemistry evolution in the northwestern part of the Amman-Al Zarqa Basin, Jordan. In this study, we collected 23 samples from the Lower Ajloun aquifer in 2021, including 1 sample from a groundwater well and 22 samples from springs. These samples were tested for electrical conductivity, total dissolved solids, pH, temperature, dissolved oxygen, the concentration of major ions (Ca^{2+}, Mg^{2+}, Na^+, K^+, HCO_3^-, Cl^-, SO_4^{2-}, and NO_3^-), and the stable isotope composition of groundwater and dissolved nitrate. The results revealed that groundwater in the study area is mainly Ca–Mg–HCO_3 type and can be classified as fresh water, hard water, and very hard water. The range and average concentration of NO_3^- were 3.5–230.8 and 50.9 mg/L, respectively. Approximately 33% of the sampling points showed NO_3^- levels above the maximum allowable concentration of 50.0 mg/L set by the World Health Organization (WHO) guidelines for drinking water quality. The values of δ^{18}O-H_2O and δ^2H-H_2O showed that groundwater in the study area is part of the current water cycle, originating in the Mediterranean Sea, with significant evaporation, orographic, and amount effects. The values of the stable isotope composition of NO_3^- corresponded to δ^{15}N-NO_3^- and δ^{18}O-NO_3^- values produced by the nitrification process of manure or septic waste and soil NH_4^+. The FA performed on the hydrochemical parameters and isotope data resulted in three main factors, with Factor 1, Factor 2, and Factor 3, accounting for 50%, 21%, and 11% of the total variance, respectively. Factor 1 was considered human-induced factor, named "pollution factor", whereas Factor 2, named "conservative fingerprint factor", and Factor 3, named "hardness factor", were considered natural factors. This study will help local researchers manage groundwater sustainably in the study area and other similar arid and semiarid areas in the world.

Keywords: stable isotope composition; δ^{15}N-NO_3^-; δ^{18}O-NO_3^-; groundwater quality; pollution sources; Jordan

Citation: Mutawakil OBEIDAT, Ahmad AL-AJLOUNI, Eman BANI-KHALED, Muheeb AWAWDEH, Muna ABU-DALO.

*Corresponding author: Mutawakil OBEIDAT (E-mail: mobeidat@just.edu.jo)
Received 2023-02-18; revised 2023-07-28; accepted 2023-08-22

2023. Integrating stable isotopes and factor analysis to delineate the groundwater provenance and pollution sources in the northwestern part of the Amman-Al Zarqa Basin, Jordan. Journal of Arid Land, 15(12): 1490–1509. https://doi.org/10.1007/s40333-023-0112-6

1 Introduction

The Sustainable Development Goal 6 (SDG 6) adopted by the United Nations in 2015 ensures accessibility to safe and affordable drinking water and sustainable management of water resources by 2030. More than 7.33×10^8 people in 2019 were living in countries with high and critical levels of water stress (UN, 2019). The vast majority of freshwater is groundwater. However, high population growth and rapid industrialization are putting strains on this valuable resource (Li and Qian, 2018; Li et al., 2022). Groundwater is critical for controlling the global water cycle, climate, and sustainability of human activities, particularly in arid environments with limited surface water resources (Tarawneh et al., 2019). Assessing groundwater quality, pollution sources, and interconnected health risks has been extensively researched in recent decades (Obeidat et al., 2012; Adimalla et al., 2020; Abascal et al., 2022).

Globally, anthropogenic nitrate is the most widespread contaminant in groundwater (Machiwal et al., 2018; Zhang et al., 2022). The problem is further complicated in arid and semiarid areas, such as Jordan, since they rely on groundwater as the ultimate source of freshwater for different purposes, in addition to a low subsurface infiltration rate and replenishment (Elmeknassi et al., 2022). According to Panno et al. (2006), the natural background of NO_3^- is typically in the range of 5.0 to 10.0 mg/L. The excessive inputs of agricultural fertilizers and manure, wastewater disposal, atmospheric inputs, leachate leakage, and groundwater overpumping have led to dramatic increases in NO_3^- levels in aquatic ecosystems, surpassing the natural background levels as well as the national and international guidelines of drinking water quality (Carrey et al., 2021; Kou et al., 2021). Intake of high doses of waterborne NO_3^- can have many negative impacts on human health (Torres-Martínez et al., 2020). Due to this prevailing concern, the World Health Organization (WHO) has set an upper NO_3^- concentration of 50.0 mg/L in drinking water (WHO, 2011). Moreover, eutrophication of standing water bodies, species extinction in river ecosystems, acidification, algal blooms, and other ecological issues are all possible outcomes of excessive nitrate inputs (Zhang et al., 2022). In addition to the environmental costs caused by nitrate pollution, the economic impacts of water contamination cannot be ignored since the remediation of contaminated water is highly costly (Obeidat et al., 2021a).

Effective management of groundwater nitrate contamination requires a solid understanding and tracing of its sources and the ongoing biochemical processes affecting its cycling (Gibrilla et al., 2020). Additionally, it requires knowledge of nitrate distribution along flow paths with a full understanding of the chemical sources and the chemical transport processes (Linhoff, 2022). A study carried out by Alam et al. (2023) revealed that farm inputs (nitrogen fertilizers and manure) are the main source of NO_3^- groundwater pollution in the rural areas of Bangladesh, contributing approximately 64% of nitrogen inputs, followed by pit latrines (18%). Accordingly, the study recommended several mitigation measures to safeguard groundwater in Bangladesh, such as the development of a nitrogen fertilizer management strategy and an increase in the educational standards of farmers to extend their awareness and understanding of the environmental impacts of the overuse of fertilizers. A field experimental study under irrigation and fertigation conditions was conducted by Su et al. (2022). The goal was to investigate the mechanisms of moisture movement, soil salinity migration, and nitrogen transformations in the soil profile. The results indicated that variations in nitrogen concentrations in the soil profile suggested that fertilizer application is the major source of nitrate in soil and groundwater. Moreover, irrigation was the main driving force for nitrogen transport and transformation in the soil. Managing groundwater nitrate problems is a constant challenge since nitrate is highly mobile, and under complex hydrogeological situations, tracing the source is quite difficult (Jung et al., 2020). As a starting point, hydrochemical data are combined with isotope data to determine groundwater flow and estimate the origin of nitrate pollution and residence time (Jia et al., 2020). The stable isotopic composition of groundwater and

nitrate have been successfully utilized for many decades to address this problem (He et al., 2022). Source identification and apportionment of nitrate, in addition to the controlling processes, have been addressed using the stable isotopic composition of nitrate. The determination of $^{18}O\text{-}NO_3^-$ and $^{15}N\text{-}NO_3^-$ helps to track the sources of nitrate in groundwater, as well as distinguish natural and synthetic fertilizers, atmospheric deposition, and sewage sources (Buzeta, 2019). This is attributed to the fact that various nitrate sources have different isotope signatures of oxygen and nitrogen (Xue et al., 2009; Gutiérrez et al., 2018). Managing water resources effectively requires the identification of pollution sources and biochemical processes affecting contaminant cycling, particularly that of nitrate (Popescu et al., 2015).

Jordan, with an approximate area of 89,210 km^2, is a country in the arid Middle East region. The majority of the country is desert, with limited and scarce water resources (Al-Kharabsheh, 2020). The country is ranked as the second most water-stressed country for renewable freshwater in the world, with approximately 61 m^3 per capita in 2021 (MWI, 2023). The crisis is worsening over time as a result of rapid population growth, agricultural expansion, increasing drought events, and climate change, as well as inefficient water use, which have placed extraordinary demands on water resources (MWI, 2023). About 70% of Jordan's water comes from groundwater extraction, of which 40%–50% is derived from nonrenewable groundwater (Salameh et al., 2014). Overpumping and low recharge rates eventually lead to groundwater depletion and deterioration of its quality (Al Wreikat and Al-Kharabsheh, 2020). High concentrations of nitrate that exceed natural background concentrations and national and international guidelines of drinking water quality have been reported in many groundwater basins in the country (Obeidat et al., 2007; Salman et al., 2014). High concentrations of nitrate in groundwater in the study area were reported by Hammouri and El-Naqa (2008). Thus, the overall objective of this study is to investigate the provenance and pollution sources of groundwater in the Amman-Al Zarqa Basin, Jordan. The specific objectives include: (1) identifying the provenance of the Lower Ajloun aquifer (the Na'ur aquifer and the Hummar aquifer) utilizing the stable isotopic composition of groundwater ($\delta^{18}O\text{-}H_2O$ and $\delta^2H\text{-}H_2O$); (2) delineating the main pollution sources based on the stable isotopic composition of dissolved nitrate ($\delta^{18}O\text{-}NO_3^-$ and $\delta^{15}N\text{-}NO_3^-$); and (3) determining the main biochemical processes affecting nitrogen species.

2 Study area

The study area is located in the northwestern part of the Amman-Al Zarqa Basin, Jordan (32°13′32″–32°20′55″N, 32°39′20″–35°56′38″E; Fig. 1). A mix of arid and Mediterranean climates dominates the basin. The winter temperature is less than 0°C, while the summer temperature is approximately 40°C (Al-Fugara et al., 2022). The average annual rainfall varies from 319 mm in the southeast to 560 mm in the north (Fig. 1b). Agricultural land accounts for approximately 33.4% of land use type, followed by urban land (29.5%), bare land (28.0%), and forest (9.0%; Fig. 1c). Table 1 presents the geological and hydrogeological classification of rock type in the study area. The Upper Cretaceous Ajloun and Belqa groups dominate the area's geology. The Lower Cretaceous Kurnub sandstones outcrop in the southern part of the study area. The Lower Cretaceous Kurnub sandstone is 300 m thick, white, and varicoloured (Bender, 1974). The Ajloun group overlies the Kurnub sandstones and comprises five formations: Na'ur (A1 and A2), Fuheis (A3), Hummar (A4), Wadi Shueib (A5 and A6), and Wadi As Sir (A7). The A1 and A2 formation consists of 150–220 m limestone interbedded with marl and marly limestone. The A3 consists of marl, marly limestone, and limestone. The A4 is 40–60 m thick and is Cenomanian in age. The A5 and A6 formation is 75–100 m thick and comprises light grey limestone and marls. The A7 comprises strongly crystalline limestone, dolomitic limestone, and chert. The Balqa group (B) comprises the Wadi Umm Ghudran (B1), Amman silicified limestone (B2), and Muwaqqar Chalk Marl (B3) formations. The B1 comprises chalk, marl, and marly limestone. The B2 has thicknesses of 80–120 m. The B3 is 60–70 m thick and is Maastrichtian in age. The aquifer systems can be separated into three primary complexes: Kurnub sandstone, Lower Ajloun (Na'ur

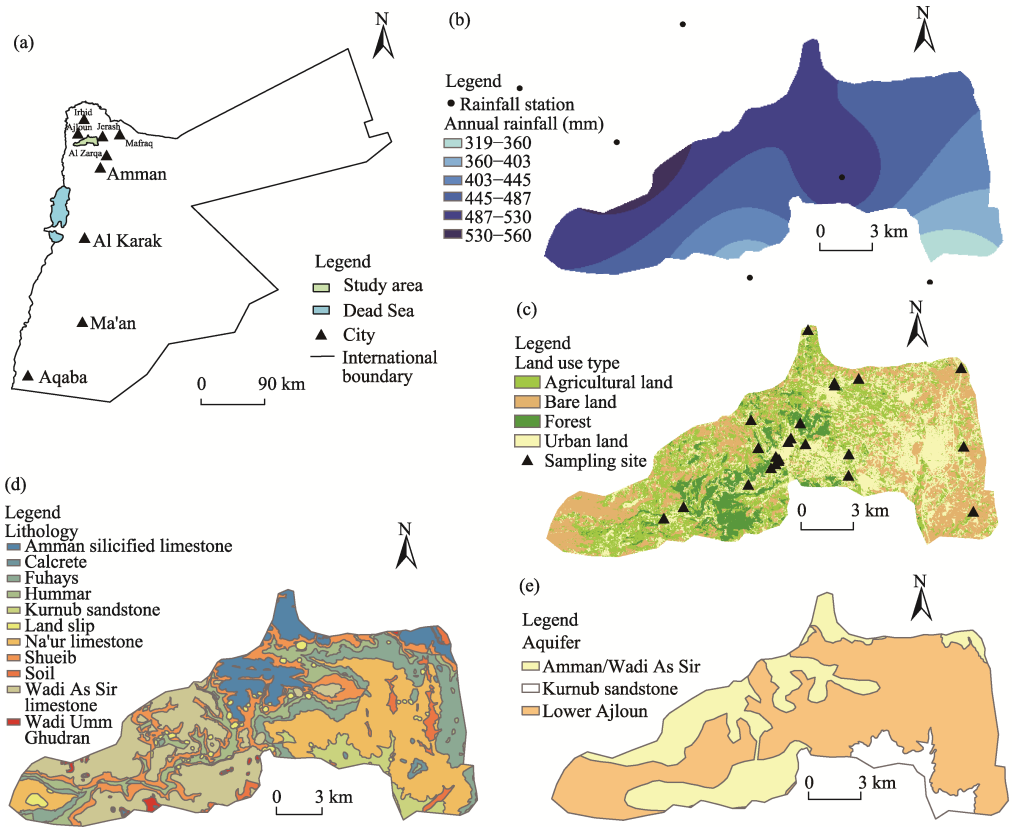

Fig. 1 Maps of the study area (a), rainfall distribution (b), land use type with sampling sites (c), the geological and hydrogeological classification of lithology (d), and aquifer systems (e)

Table 1 Geological and hydrogeological classification of rock type in the Amman-Al Zarqa Basin

Epoch	Stage	Group	Formation	Symbol	Thickness (m)	Rock type	Aquifer potentiality	Permeability (m/s)
Upper Cretaceous	Maastrichtian	Balqa	Muwaqqar Chalk Marl	B3	60–70	Chalk, marl, and chalky limestone	Poor	-
	Campanian		Amman silicified limestone	B2	80–120	Chert and limestone with phosphate	Excellent	1.0×10^{-5}–3.0×10^{-4}
	Santonian		Wadi Umm Ghudran	B1	15–20	Chalk, marl, and marly limestone	Poor	-
	Turonian	Ajloun	Wadi As Sir	A7	90–110	Hard crystalline limestone and dolomitic and some chert	Excellent	1.0×10^{-7}–1.0×10^{-4}
			Shueib	A5 and A6	75–100	Light grey limestone interbedded with marls and marly limestone	Fair to poor	6.3×10^{-5}–7.2×10^{-4}
			Hummar	A4	40–60	Hard dense limestone and dolomitic limestone	Good	8.1×10^{-7}–7.3×10^{-4}
			Fuhays	A3	60–80	Grey and olive-green soft marl, marly limestone, and limestone	Poor	5.3×10^{-7}–1.7×10^{-5}
	Cenomanian		Na'ur	A1 and A2	150–220	Limestone interbedded with a thick sequence of marl and marly limestone	Poor	2.0×10^{-8}–3.1×10^{-5}
Lower Cretaceous	Albian Aptian		Kurnub	K	300	Massive white and varicoloured sandstone with layers of reddish silt and shale	Good	6.9×10^{-3}–5.2×10^{-2}

Note: "-" means no data. This table is referenced from Rimawi (1985).

and Hummar), and Amman/Wadi As Sir (Fig. 1e). The Kurnub sandstone aquifer is a potentially useful aquifer in Jordan; however, in the study area, the aquifer is uneconomic, and its groundwater quality is poor (Hammouri and El-Naqa, 2007). The Na'ur aquifer is made of limestone and marl and overlies the Kurnub sandstone. Al-Alawneh (1998) estimated the mean annual recharge of the aquifer at approximately 4.5×10^6 m^3. The specific capacity, transmissivity, and hydraulic conductivity values of the Na'ur aquifer are 0.01–12.00 m^3/h, 0.3–100.0 m^2/d, and 0.003–2.700 m/d, respectively (Salameh and Bannayan, 1993). The Hummar aquifer is made of hard, crystalline, coarse-grained, and fractured dolomitic limestone. The transmissivity of the Hummar aquifer is 32.0–300.0 m^2/d. The permeability of this aquifer ranges from 8.1×10^{-7} to 7.3×10^{-4} m/s (Rimawi, 1985), with 5.0×10^6 to 6.0×10^6 m^3/a of recharge (Al-Alawneh, 1998). The Wadi As Sir is the most important aquifer in the basin, with a permeability of 1.0×10^{-7}–1.0×10^{-4} m/s and a transmissivity of 10.0–6300.0 m^2/d (Al Mahamid, 2005).

3 Materials and methods

3.1 Sampling and fieldwork

In this study, we collected 23 groundwater samples from the Lower Ajloun aquifer (the Na'ur aquifer and the Hummar aquifer) in March 2021, including 1 sample from a groundwater well and 22 samples from springs (Fig. 1c). These samples were collected at the mouths of springs. Prior to sampling, the sampling well was purged to ensure that the groundwater samples accurately represent the subsurface environment features and circumstances. Electrical conductivity (EC), pH, total dissolved solids (TDS), and temperature were measured in situ using a portable meter (Elite PCTS, Thermo Scientific, Waltham, USA), and dissolved oxygen (DO) was measured using a DO meter (SensoDirect 150, Lovibond, Dortmund, Germany). Before laboratory examination, all groundwater samples were filtered and transferred to prewashed low-density polyethylene bottles. The samples for chemical analysis were kept in a refrigerator, while the samples for $^{15}N\text{-}NO_3^-$ and $^{18}O\text{-}NO_3^-$ determination were frozen before being shipped to the Environmental Isotope Laboratory of University of Waterloo, Canada, for analysis. The samples for $\delta^2H\text{-}H_2O$ and $\delta^{18}O\text{-}H_2O$ determination were collected in 50-mL bottles and stored at room temperature until transported to the Environmental Isotope Laboratory of University of Waterloo, Canada. The procedures of fieldwork and laboratory work are based on APHA (1998). We used global position system (GPS map 60CSx, Garmin Ltd., Kansas, USA) to get the coordinates of these samples.

3.2 Laboratory chemical analyses

The concentrations of Na^+, K^+, Ca^{2+}, Mg^{2+}, and Cl^- were determined using an ion chromatograph (Dionix ICS-1600, Thermo Fisher Scientific, Sunnyvale, USA). The concentrations of SO_4^{2-} and NO_3^- were determined using a spectrophotometer (Lovibond 712005, Spectro Direct, Dortmund, Germany). The HCO_3^- concentration was determined by the titration method. The total hardness (TH; mg/L) was determined using the following formula (Todd, 1980):

$$TH = 2.497(Ca^{2+}) + 4.11(Mg^{2+}), \tag{1}$$

where Ca^{2+} (mg/L) and Mg^{2+} (mg/L) represent the concentrations of Ca^{2+} and Mg^{2+}, respectively.

The analytical uncertainty was less than 4%, and the samples were analysed in triplicate. In order to verify the correctness of the analysis, we used the anion-cation balance method; it was reproducible within ±10% error limits (Appelo, 2005):

$$\text{Error} = \frac{\sum \text{cations} - \sum \text{anions}}{\sum \text{cations} + \sum \text{anions}} \times 100\%, \tag{2}$$

where Σcations is the total ionic concentration of cations (mol/L); and Σanions is the total ionic concentration of anions (mol/L).

3.3 Stable isotope composition

The $^{15}N/^{14}N$ and $^{18}O/^{16}O$ of NO_3^-, as well as the $^{18}O/^{16}O$ and $^{2}H/^{1}H$ of water were determined at

the Environmental Isotope Laboratory of University of Waterloo, Canada. The $^{15}N/^{14}N$ and $^{18}O/^{16}O$ of NO_3^- were determined using a N_2O chemical denitrifier (GVI Trace Gas Iso Prime, Elemental Microanalysis, Okehampton, UK) and following the technique described by Mcilvin and Altabet (2005). The analytical precision of $^{15}N/^{14}N$ and $^{18}O/^{16}O$ of NO_3^- in the laboratory analysis was ±0.3 and ±0.8, respectively. A liquid water isotope analyser (T-LWIA-45-EP, Los Gatos Research, California, USA) was utilized to determine the $^{18}O/^{16}O$ and $^{2}H/^{1}H$ of water, with analytical precisions of ±0.2 and ±0.8 for ^{18}O and ^{2}H, respectively. The ratios are calculated using the following formula:

$$\delta_{\text{sample}} = \left(\frac{R_{\text{sample}} - R_{\text{standard}}}{R_{\text{standard}}} \right) \times 1000‰ , \tag{3}$$

where δ_{sample} (‰) and R_{sample} are the $^{15}N/^{14}N$, $^{2}H/^{1}H$, or $^{18}O/^{16}O$ of the sample and the international reference, respectively; and R_{standard} is the $^{15}N/^{14}N$, $^{2}H/^{1}H$, or $^{18}O/^{16}O$ of the standard sample. The international reference used to report the values of $\delta^{15}N$ is N_2 in atmospheric air, whereas Vienna Standard Mean Ocean Water (VSMOW) is used to report $\delta^{18}O$ and $\delta^{2}H$ values.

3.4 Chloro-alkaline index (CAI)

The CAI has been widely used to investigate the ion exchange processes in groundwater (Toumi et al., 2015). The CAI can be calculated using the following equation (Schoeller, 1977):

$$\text{CAI} = \frac{Cl^- - (Na^+ + K^+)}{Cl^-}, \tag{4}$$

where Cl^- (mol/L), Na^+ (mol/L), and K^+ (mol/L) represent the concentrations of Cl^-, Na^+, and K^+, respectively.

3.5 Principal component analysis (PCA) and factor analysis (FA)

PCA is a multivariate statistical technique that is widely used in groundwater quality assessment studies (Obeidat et al., 2013; Wu et al., 2014). In this study, we used PCA to analyse the main hydrochemical and isotopic data of groundwater. A total of 14 parameters were involved in the analysis, including the concentration of major ions, EC, TDS, pH, temperature, DO, and the stable isotope composition of groundwater and dissolved nitrate. To check the appropriateness of the data for PCA, we used the Kaiser-Meyer-Olkin (KMO) test, and the result is 0.726 (>0.500), indicating that the data are suitable for PCA. Moreover, the value of Bartlett test is 0.00, which is smaller than 0.05, indicating that PCA can be applied successfully. An eigenvalue greater than 1.00 is the basis for variable selection. To maximize the sum of variance of the factors coefficients, we employed varimax rotation to better understand and infer the processes and factors influencing groundwater chemistry. SPSS 13 software was utilized to carry out PCA and FA.

4 Results and discussion

4.1 General hydrochemistry

The physiochemical parameters of groundwater depend on rock weathering, the quality of recharge water, ion exchange, leakage from the river base, evaporation, and human activities. Exploring groundwater chemistry helps to evaluate the hydrogeochemical features of water resources and assess groundwater quality suitability for irrigation and drinking (Rezaei et al., 2020; Ren et al., 2021). Table 2 presents the descriptive statistics of the hydrochemical parameters of groundwater in the study area, as well as these parameters reported by the WHO (2011) and Jordan Standards and Metrology Organization (2015).

According to Table 2, we found that K^+ has the highest coefficient of variation (CV), followed by NO_3^-, Cl^-, Na^+, SO_4^{2-}, and Mg^{2+}. This indicates diverse sources and processes governing the spatial distribution of these ions. The lowest CV was HCO_3^- (19.6%), which may indicate a single source. Ca^{2+} was the dominant cation, followed by Mg^{2+}, Na^+, and K^+. The dominant anion was HCO_3^-, followed by Cl^-, NO_3^-, and SO_4^{2-}. The pH values were in the range of 7.3–8.6, with an

Table 2 Descriptive statistics of the hydrochemical parameters of groundwater in the study area

Parameter	Minimum	Maximum	Mean	Standard deviation	CV (%)	WHO (2011)	Jordan Standards and Metrology Organization (2015)
pH	7.3	8.6	7.7	0.4	5.2	6.5–8.5	6.5–9.0
Temperature (°C)	13.6	21.6	17.9	1.5	8.4	12.0–25.0	12.0–25.0
TDS (mg/L)	324.0	1030.0	539.3	163.8	30.4	500.0–1000.0	500.0–1500.0
EC (μS/cm)	457.0	1423.0	758.9	228.2	30.1	1500.0	1500.0
TH (mg/L)	152.4	426.4	57.4	13.0	22.6	300.0–500.0	300.0–500.0
DO (mg/L)	4.6	11.6	7.5	1.3	16.9	-	-
Na^+ (mg/L)	10.3	80.5	26.8	18.6	69.4	150.0–200.0	200.0–400.0
K^+ (mg/L)	0.1	26.0	2.6	5.4	200.1	10.0–20.0	10.0–50.0
Mg^{2+} (mg/L)	5.9	32.3	14.0	7.7	55.0	50.0–100.0	50.0–150.0
Ca^{2+} (mg/L)	44.3	156.0	81.9	23.7	28.9	75.0–100.0	75.0–200.0
SO_4^{2-} (mg/L)	13.0	117.7	33.4	22.4	67.1	200.0–250.0	200.0–500.0
Cl^- (mg/L)	14.2	139.1	47.2	36.0	76.3	200.0–250.0	200.0–500.0
HCO_3^- (mg/L)	64.0	128.0	96.9	19.0	19.6	125.0–350.0	100.0–500.0
NO_3^- (mg/L)	3.5	230.8	50.9	56.4	100.1	45.0–50.0	50.0–70.0

Note: TDS, total dissolved solids; EC, electrical conductivity; TH, total hardness; DO, dissolved oxygen; CV, coefficient of variation. "-" means no data.

average of 7.7, indicating that the groundwater in the study area is slightly alkaline. The pH values of all samples were within the range reported by WHO (2011) and Jordan Standards and Metrology Organization (2015). The DO ranged from 4.6 to 11.6 mg/L, with an average of 7.5 mg/L. The TDS was in the range of 324.0–1030.0 mg/L, with an average of 539.3 mg/L.

The EC values were in the range of 457.0–1423.0 μS/cm, with an average of 758.9 μS/cm (Fig. 2). All EC values were within the permissible limits of WHO (2011) and Jordan Standards and Metrology Organization (2015) for drinking water quality. The TH values ranged from 152.4 to 426.4 mg/L. Accordingly, groundwater can be classified as hard to very hard water. Ca^{2+} enters the aquatic environment predominantly through the weathering of rocks rich in calcium compounds, such as limestone, which is dominant in the study area (Meybeck, 1987). An additional source of Ca^{2+} is agricultural fertilizer (Weyhenmeyer et al., 2019). The Ca^{2+} concentrations were in the range of 44.3–156.0 mg/L, with an average of 81.9 mg/L. Approximately 57% of the samples showed Ca^{2+} concentrations that exceeded the maximum Ca^{2+} concentration set by WHO (2011). However, based on Jordan Standards and Metrology Organization (2015), all groundwater samples were considered safe. The range and average Mg^{2+} concentrations were 5.9–32.3 and 14.0 mg/L, respectively, and the Na^+ concentrations were in the range of 10.3–80.5 mg/L, with an average of 26.8 mg/L. None of the samples exceeded the maximum Mg^{2+} and Na^+ concentrations set by WHO (2011) and Jordan Standards and Metrology Organization (2015). Magnesium and sodium in groundwater originate from the decomposition of carbonate minerals, silicates, evaporates, and air input (Afroza et al., 2009). Agricultural operations and sewage effluents may be additional sources of sodium in groundwater (Hem, 1985). The K^+ concentrations were in the range of 0.1–26.0 mg/L. The HCO_3^- concentrations varied from 64.0 to 128.0 mg/L, with an average of 96.9 mg/L. The Cl^- concentrations ranged from 14.2 to 139.1 mg/L, with an average of 47.2 mg/L, and the SO_4^{2-} concentrations were in range of 13.0–117.7 mg/L, with an average of 33.4 mg/L. Chlorides and sulfates in groundwater come from water–rock interactions, seawater encroachment, industrial waste, or home sewage (Venkatesan et al., 2021). The concentrations of HCO_3^-, Cl^-, and SO_4^{2-} in all groundwater samples met the drinking water quality standard of WHO (2011) and Jordan Standards and Metrology Organization (2015). The NO_3^- concentrations varied from 3.5 to 230.8 mg/L, with an average of 50.9 mg/L (Fig. 2b). We divided the NO_3^- concentrations into three categories. Firstly, NO_3^- concentration is less than 10.0 mg/L; this

category involves those samples having NO_3^- concentrations with low risk to humans and aquatic ecosystems and covers 4% of the samples. Secondly, NO_3^- concentrations are in range of 10.0–50.0 mg/L, indicating the impacts of human activities; this category involves 61% of the samples. Thirdly, NO_3^- concentrations are higher than 50.0 mg/L, exceeding the drinking water quality reported by WHO (2011); this category comprises 35% of the samples. The results showed that the EC is significantly positively correlated with TDS, NO_3^-, Cl^-, SO_4^{2-}, Na^+, and Ca^{2+} (Table 3), indicating that groundwater chemistry is substantially influenced by processes and activities involving these parameters. Furthermore, the results also demonstrated that NO_3^- is significantly correlated with Cl^- and SO_4^{2-}, indicating a common source of these ions, such as fertilizers, sewage, and animal waste.

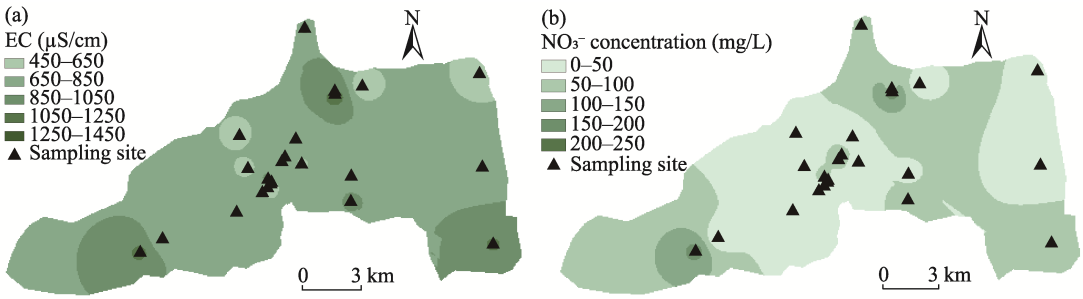

Fig. 2 Spatial distribution of electrical conductivity (EC; a) and NO_3^- concentration (b)

Table 3 Pearson correlation coefficients for the major hydrochemical parameters of groundwater in the study area

Parameter	Ca^{2+}	Mg^{2+}	Na^+	K^+	HCO_3^-	SO_4^{2-}	NO_3^-	Cl^-	EC	TH	TDS
Ca^{2+}	1.00	0.77**	0.58**	0.20	0.34**	0.57**	0.60**	0.76**	0.85**	0.94**	0.90**
Mg^{2+}	0.77**	1.00	0.53**	0.43**	0.10	0.50**	0.40**	0.80**	0.85**	0.94**	0.84**
Na^+	0.58**	0.53**	1.00	0.36**	–0.10	0.87**	0.60**	0.84**	0.85**	0.59**	0.78**
K^+	0.20	0.43**	0.36**	1.00	–0.40	0.27*	–0.10	0.50**	0.42**	0.31**	0.34**
HCO_3^-	0.34**	0.10	–0.10	–0.40	1.00	–0.10	0.20	–0.20	0.10	0.22*	0.29**
SO_4^{2-}	0.57**	0.50**	0.87**	0.27*	–0.10	1.00	0.67**	0.78**	0.78**	0.58**	0.69**
NO_3^-	0.60**	0.38**	0.60**	–0.10	0.20	0.67**	1.00	0.54**	0.62**	0.52**	0.62**
Cl^-	0.76**	0.80**	0.84**	0.50**	–0.20	0.78**	0.54**	1.00	0.95**	0.83**	0.86**
EC	0.85**	0.85**	0.85**	0.42**	0.10	0.78**	0.62**	0.95**	1.00	0.90**	0.95**
TH	0.94**	0.94**	0.59**	0.31**	0.22*	0.58**	0.52**	0.83**	0.90**	1.00	0.92**
TDS	0.90**	0.84**	0.78**	0.34**	0.29**	0.69**	0.62**	0.86**	0.95**	0.92**	1.00

Note: *, $P<0.05$ level; **, $P<0.01$ level.

4.2 Natural processes contributing to the groundwater chemical composition

The Piper diagram is a common tool for deducing hydrochemical facies and processes that influence water chemistry. We can see from Figure 3 that, in the study area, the Ca-Mg-HCO_3 type covers 44% of the samples, followed by the Ca-Mg-Cl type (39%) and Ca-Mg-SO_4 type (17%). The first type is a reflection of the primary rock formations in the region, which include limestone and dolomite, and presents freshwater that has been recently recharged and has not been contaminated by human activity (El Yaouti et al., 2009). The Ca-Mg-Cl type can be interpreted as water that results from the mixing of highly saline solutions, such as domestic wastewater with uncontaminated freshwater, followed by ion exchange processes (Selvam et al., 2016).

Although the Gibbs diagram was initially developed to explain the mechanisms controlling surface water chemistry, such as evaporation, weathering, and precipitation (Gibbs, 1970), it has been extensively applied in groundwater hydrochemistry (Liu et al., 2023; Samtio et al., 2023; Yang et al., 2023; Zhang et al., 2023). The Gibbs diagram can also be applied in groundwater studies and can lead to a better understanding of the main driving hydrochemical processes

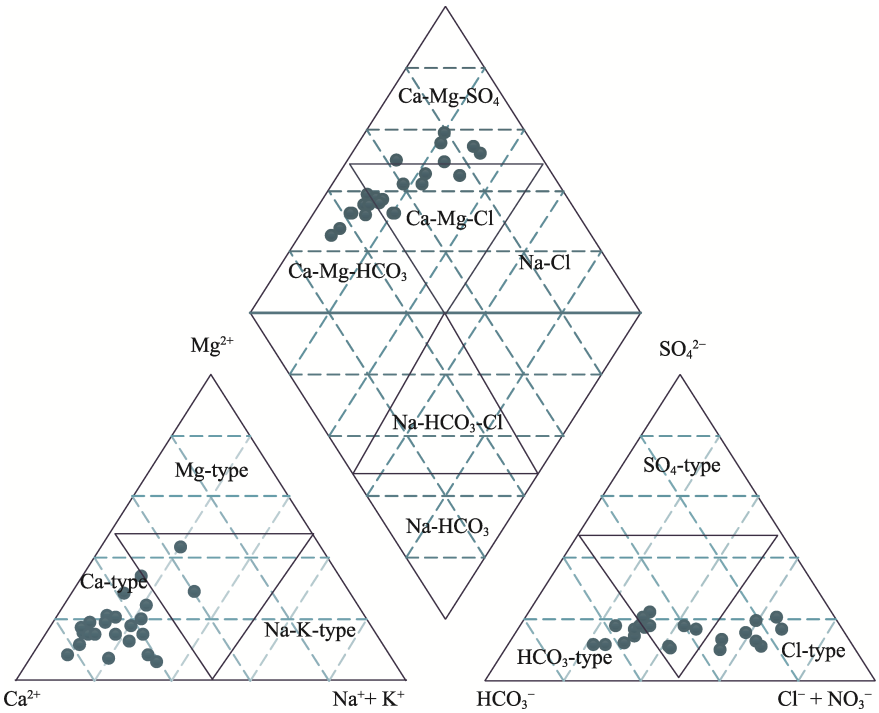

Fig. 3 Piper diagram showing different hydrochemical facies of groundwater in the study area

(Marandi and Shand, 2018), since approximately two-thirds of global streamflow stems from delayed flows such as groundwater (Jasechko et al., 2016). Additionally, the hydrochemical processes can be better understood by integrating Gibbs diagrams with other tools, such as Piper diagrams and analytes (Marandi and Shand, 2018). The Gibbs diagram revealed that all samples from the study area are located in the rock dominance zone (Fig. 4), indicating that rock weathering is the main natural process contributing to groundwater hydrochemistry. Furthermore, it can be seen from Figure 4 that evaporation is not a dominant process affecting groundwater hydrochemistry, which is also confirmed by the negative correlations between Na^+ and TDS and between Cl^- and TDS. The study conducted by Sajil Kumar and James (2016) showed that evaporation leads to an increase in TDS when Na^+ or Cl^- is constant. A Chadha diagram was utilized to classify natural waters and identify hydrogeochemical processes controlling water quality (Chadha, 1999). According to this diagram, we can divide the groundwater of the study area into two fields (Fig. 5): (1) the recharge water field, which is the Ca-Mg-HCO_3 type, with approximately 35% of the samples distributed in this field; and (2) the ion exchange field, which demonstrates the Ca-Mg-Cl type, with approximately 65% of the samples distributed in this field. The former type indicates that alkaline earths and weak acidic anions exceed alkalis and strong acidic anions, and this type has temporary hardness (Chadha, 1999). On the other hand, the ion exchange field represents alkaline earths exceeding alkali metals and strong acidic anions exceeding weak acidic anions, and this type has permanent hardness (Barzegar et al., 2017). We found two types of exchange processes: (1) reverse ion exchange, where Ca^{2+} and Mg^{2+} in the host aquifer are replaced by Na^+ and K^+ in water, leading to the hardening of groundwater (Zaidi et al., 2015; Abu-Alnaeem et al., 2018; Tiwari et al., 2019); and (2) base ion exchange, where K^+ and Na^+ in the host aquifer are replaced by Ca^{2+} and Mg^{2+} in water, eventually leading to the softening of groundwater. In the study area, about 52% of the samples had a negative CAI value, while about 28% had a positive CAI value (Fig. 5c).

The presence of both types of CAI indicated that both types of ongoing ion exchange processes affect groundwater chemistry. However, the CAI values were in the range of –0.20 to 0.36 signifying that the ion exchange process is not as intense. Furthermore, the relationship of

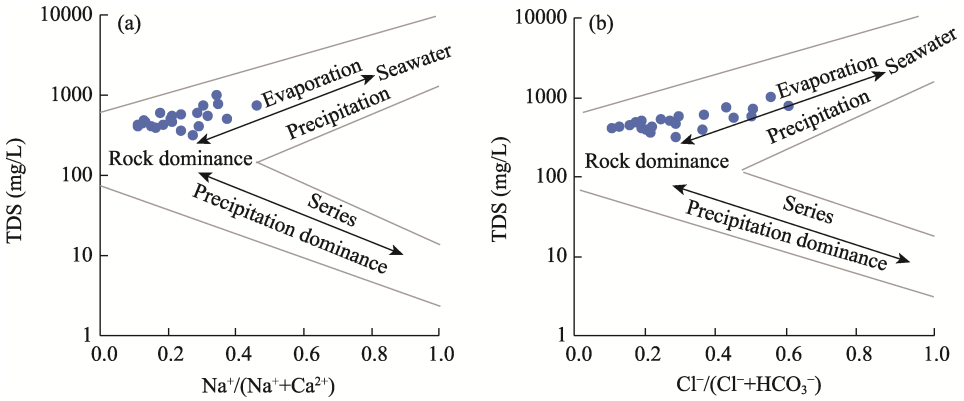

Fig. 4 Gibbs diagram of the main processes controlling groundwater chemistry in the study area. (a), $N^+/(Na^++Ca^{2+})$ vs. total dissolved solids (TDS); (b), $Cl^-/(Cl^-+HCO_3^-)$ vs. TDS.

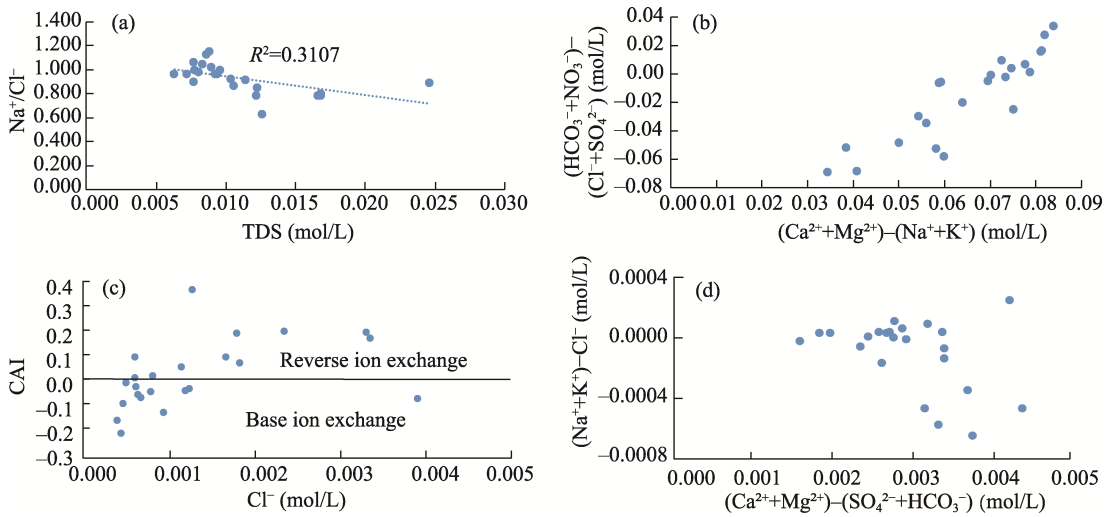

Fig. 5 Plot of TDS vs. Na^+/Cl^- (a), Chadha diagram of groundwater samples (b), plot of Cl^- vs. Chloro-alkaline index (CAI; c), and plot of $(Na^++K^+)–Cl^-$ vs. $(Ca^{2+}+Mg^{2+})–(SO_4^{2-}+HCO_3^-)$ (d). In Figure 5c, the black solid line separates the two types of ion exchange (reverse ion exchange and base ion exchange).

$(Ca^{2+}+Mg^{2+})–(SO_4^{2-}+HCO_3^-)$ with $(Na^++K^+)–Cl^-$ was applied to evaluate and validate the role of cation exchange processes in groundwater chemistry. By using the aforementioned relationship, it is found that ion exchange is a fundamental process affecting the groundwater chemistry in the study area (Fig. 5d). Additionally, the relationship between $Ca^{2+}+Mg^{2+}$ and $HCO_3^-+SO_4^{2-}$ indicated an ion exchange process since most of the samples are below the 1:1 reference line (Fig. 6). The ratio of HCO_3^- to Cl^- is a good indicator of groundwater salinization (Ayadi et al., 2018). Most of the samples (approximately 70%) in the study area had a ratio of HCO_3^- to Cl^- greater than 1.0, indicating freshwater recharge. To infer carbonate mineral dissolution, we analyzed the relationship between Cl^- and Ca^{2+}/HCO_3^- of groundwater (Fig. 6b). Abu-Alnaeem et al. (2018) showed that if calcite dissolution is the dominant process, the ratio of Ca^{2+}/HCO_3^- to Cl^- should be approximately 1.0; if dolomite dissolution is the prevailing process, the value should be about 0.5. Clearly, all samples had the ratio of Ca^{2+}/HCO_3^- to Cl^- greater than 1.0, indicating that the ion exchange process affects groundwater chemistry. As depicted in Figure 6c, there was a significant linear relationship (r=0.87; P<0.01) between $(NO_3^-+Cl^-)/HCO_3^-$ and TDS, indicating that human activities have impacted groundwater chemistry in the study area (Jalali, 2009). This was confirmed by the significant correlation between NO_3^- and Cl^-, indicating that domestic wastewater is a primary source of groundwater pollution in the study area (Reddy et al., 2009).

Table 4 shows the PCA results of the hydrochemical parameters, δ^2H-H_2O, $\delta^{18}O$-H_2O,

$\delta^{15}N\text{-}NO_3^-$, and $\delta^{18}O\text{-}NO_3^-$. Factor 1 accounted for 50% of the total variance and had strong positive loadings on EC, Cl^-, SO_4^{2-}, NO_3^-, Na^+, K^+, Ca^{2+}, and $\delta^{15}N\text{-}NO_3^-$. The association of these parameters clearly indicated the anthropogenic impacts on groundwater quality, and hence, it was termed "pollution factor". Infiltration of domestic wastewater frequently causes an increase in hydrochemical parameter levels, such as TDS, Na^+, Ca^{2+}, K^+, Cl^-, and NO_3^- (Wang et al., 2017; Zhu et al., 2019). The connection between NO_3^- and SO_4^{2-} demonstrated that synthetic fertilizers and domestic wastewater have an impact on groundwater quality (Das and Nag, 2017; Aravinthasamy et al., 2020). Factor 2 accounted for 21% of the total variance, exhibiting strong positive loadings on $\delta^2H\text{-}H_2O$, $\delta^{18}O\text{-}H_2O$, and $\delta^{18}O\text{-}NO_3^-$. It was named "conservative fingerprint factor". The association of $\delta^{18}O\text{-}NO_3^-$ with $\delta^2H\text{-}H_2O$ and $\delta^{18}O\text{-}H_2O$ ascertained the presence of nitrification since $\delta^{18}O\text{-}NO_3^-$ generated by bacterial nitrification should have two oxygen atoms from groundwater and one oxygen atom from the air (Kendall et al., 2007). Factor 3 accounted for 11% of the total variance and had very strong loadings on Mg^{2+} and HCO_3^-. The factor can be termed "hardness factor" since Mg^{2+} is a major component of water hardness. The association of magnesium and bicarbonate reflects freshwater recharge and water–rock interaction (Prasanna et al., 2010).

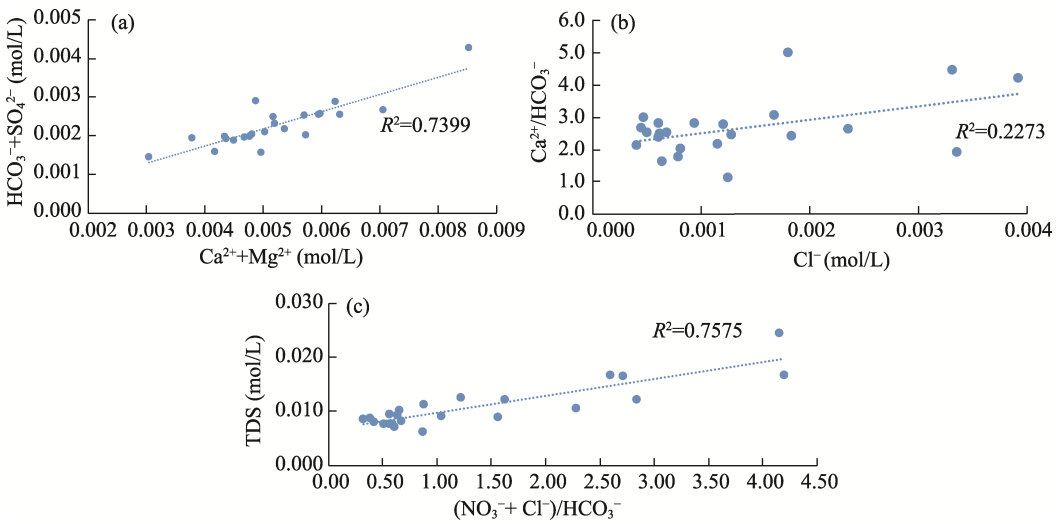

Fig. 6 Relationships between $Ca^{2+}+Mg^{2+}$ and $HCO_3^-+SO_4^{2-}$ (a), Cl^- and Ca^{2+}/HCO_3^- (b), and $(NO_3^-+Cl^-)/HCO_3^-$ and TDS (c)

4.3 Stable isotope composition of groundwater ($\delta^2H\text{-}H_2O$ and $\delta^{18}O\text{-}H_2O$)

Meteorological factors, including temperature and rainfall amount, continental effect, altitude, and latitude strongly affect the stable isotope composition of water. Both δ^2H and $\delta^{18}O$ are widely used to better understand temporal and geographical isotope variability trends in precipitation (Rozanski et al., 1993; Dutton et al., 2005). Table 5 shows that $\delta^{18}O$ varied from –7.0‰ to –5.9‰, with an average of –6.7‰, and δ^2H ranged from –32.5‰ to –26.6‰, with an average of –29.7‰. We plotted the relationship between δ^2H and $\delta^{18}O$ (Fig. 7) alongside the global meteoric water line (GMWL), Mediterranean meteoric water line (MMWL), and local meteoric line (LMWL) of Jordan (Bajjali, 2012). The closeness of the groundwater samples to the LMWL and the MMWL indicated that groundwater has been replenished by Mediterranean water. We divided the groundwater samples into two groups. The first group (21 samples) had $\delta^{18}O$ and δ^2H values in the ranges of –7.0‰ to –6.4‰ and –32.5‰ to –27.5‰, respectively. All samples were plotted between the LMWL and the MMWL, indicating a common origin, which is the Mediterranean meteoric water. The second group (two samples) had $\delta^{18}O$ and δ^2H values in the ranges of –5.9‰ to–5.8‰ and –26.6‰ to –27.9‰, respectively. The two samples were between the MMWL and the GMWL, indicating that they are recharged by a mix of two sources; they were $\delta^{18}O$-enriched compared to the first group. The study area is located in the Mediterranean bioclimatic region,

Table 4 Principal component analysis (PCA) of the hydrochemical parameters, δ^2H-H_2O, δ^{18}O-H_2O, δ^{15}N-NO_3^-, and δ^{18}O-NO_3^-

Parameter	Factor 1	Factor 2	Factor 3
Cl^-	0.93	0.25	0.10
NO_3^-	0.95	0.15	0.01
SO_4^{2-}	0.95	–0.06	0.08
HCO_3^-	0.10	–0.03	0.88
Na^+	0.94	0.25	0.10
K^+	0.80	–0.08	0.08
Mg^{2+}	0.05	0.34	0.85
Ca^{2+}	0.80	–0.23	–0.17
EC	0.95	0.06	0.21
δ^{18}O-H_2O	0.14	0.87	0.28
δ^2H-H_2O	–0.01	0.86	–0.16
δ^{15}N-NO_3^-	0.75	–0.04	0.02
δ^{18}O-NO_3^-	–0.03	0.79	0.21
Eigenvalue	6.46	2.70	1.37
Percentage of variance (%)	49.65	20.78	10.51
Cumulative percentage of variance (%)	49.65	70.43	80.94

Note: Factor 1, Factor 2, and Factor 3 represent pollution factor, conservative fingerprint factor, and hardness factor, respectively.

which is characterized by an abundance of precipitation during the cool, wet winter season and a highly pronounced summer drought (Bajjali, 2012). According to Kattan (2019), the sources of air masses generating precipitation over the Middle East stem from a variety of locations, including the Atlantic Ocean, the North Pole via Eastern Europe, the Siberian Plateau, North Africa, and the Red Sea. All samples had *d*-excess values between 19.1‰ and 25.6‰, with an average of 23.6‰. These values were consistent with the *d*-excess values of the rainfall from central and northern Jordan, which varied from 23.0‰ to 25.6‰. A significant inverse correlation (r= –0.76; P<0.01) was found in the relationship between δ^{18}O and *d*-excess, indicating an evaporation effect on groundwater isotopic composition. An orographic effect on the stable isotope composition of groundwater was also found, where a significant negative correlation (r= –0.76; P<0.01) between δ^{18}O and altitude was detected. The depletion of δ^{18}O values was –0.2‰ δ^{18}O per 100 m, which is consistent with the global average depletion of δ^{18}O with altitudes of –0.15‰ to –0.50‰ δ^{18}O () per 100 m (Aeschbach-Hertig et al., 2007). Furthermore, a significant negative correlation (r= –0.61; P< 0.01) between δ^{18}O and rainfall amount was found. According to Bajjali (2012), the eastern highlands of Jordan Rift Valley prevent air masses from crossing the Mediterranean and pushing them upwards.

The relationship between stable isotopes and TDS can be used to delineate processes governing groundwater chemistry (Liu et al., 2023). In particular, δ^{18}O and *d*-excess can reveal the contributions of mineral dissolution, evaporation, and precipitation (Qu et al., 2023). The *d*-excess values decrease during evaporation and remain constant during mineral dissolution (Dansgaard, 1964). Moreover, δ^{18}O might increase significantly during evaporation, decrease under mixing with rainwater, and increase slightly or remain constant during mineral dissolution (Qu et al., 2023). As presented in Figure 8, most of the samples showed no significant changes in *d*-excess and δ^{18}O with increasing TDS, signifying mineral dissolution or other sources of groundwater salinity in the study area. The relationship between TDS and NO_3^- showed a trend covariation, indicating an anthropogenic source of the groundwater salinity (Fig. 8).

4.4 Stable isotope composition of dissolved nitrate (δ^{15}N-NO_3^- and δ^{18}O-NO_3^-)

The stable isotope composition of dissolved nitrate (δ^{15}N and δ^{18}O) has emerged as a powerful aid for tracing nitrate sources and cycling processes in groundwater, as various sources of nitrate

Table 5 Stable isotopic composition of groundwater samples

Sampling site	NO_3^- (mg/L)	$\delta^{18}O$-H_2O-VSMOW (‰)	$\delta^{2}H$-H_2O-VSMOW (‰)	*d*-excess (‰)	$\delta^{15}N$-NO_3^--atmospheric air (‰)	$\delta^{18}O$-NO_3^--VSMOW (‰)	Theoretical $\delta^{18}O$-NO_3^- (‰)
1	54.3	–6.64	–30.40	22.76	7.37	1.49	2.60
2	24.1	–6.91	–31.19	24.09	6.20	3.05	2.42
3	13.8	–6.72	–31.71	22.05	3.72	2.64	2.55
4	230.8	–6.61	–30.10	22.75	11.26	2.33	2.62
5	10.3	–6.95	–30.43	25.20	2.56	1.35	2.39
6	73.4	–6.97	–30.92	24.82	10.97	1.47	2.38
7	63.2	–7.01	–30.96	25.11	11.34	2.15	2.35
8	120.3	–6.86	–29.92	24.95	13.67	2.85	2.46
9	12.1	–6.79	–29.63	24.65	3.29	2.70	2.50
10	31.1	–6.55	–28.63	23.81	4.98	1.94	2.66
11	20.2	–6.55	–28.27	24.14	6.63	2.71	2.66
12	164.4	–6.38	–27.73	23.31	8.35	2.58	2.78
13	16.2	–6.88	–30.73	24.27	4.30	2.52	2.44
14	14.7	–6.85	–30.61	24.19	2.88	1.82	2.46
15	18.1	–6.90	–30.88	24.33	7.42	1.13	2.43
16	43.5	–6.48	–30.22	21.63	8.95	3.13	2.71
17	72.5	–6.50	–30.09	21.88	10.16	4.32	2.70
18	97.4	–5.87	–27.92	19.07	8.15	7.40	3.12
19	3.5	–6.78	–32.52	21.74	7.25	3.47	2.51
20	46.7	–5.96	–26.62	21.09	3.88	4.29	3.05
21	14.8	–6.72	–28.34	25.40	4.82	5.48	2.55
22	14.1	–6.69	–28.60	24.91	5.53	5.31	2.57
23	12.4	–6.64	–27.52	25.64	8.39	3.63	2.60
Maximum	230.8	–5.90	–26.60	25.60	13.70	7.40	3.10
Minimum	3.5	–7.00	–32.50	19.10	2.60	1.10	2.40
Average	50.9	–6.70	–29.70	23.60	7.00	3.00	2.60

Note: VSMOW is Vienna Standard Mean Ocean Water.

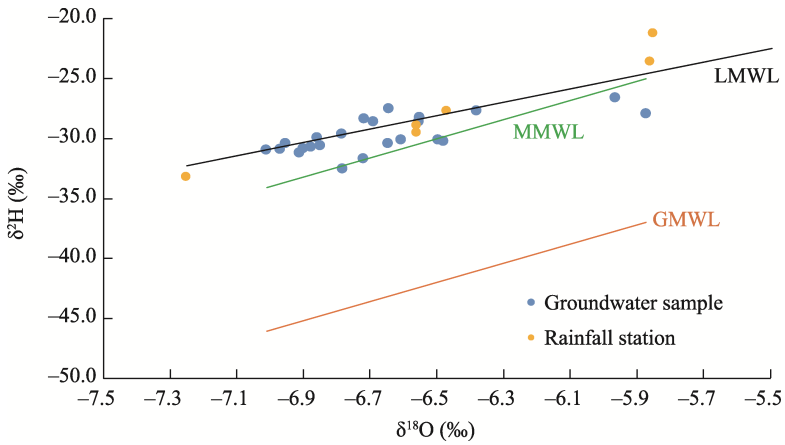

Fig. 7 Relationship between $\delta^{18}O$ and $\delta^{2}H$ of groundwater samples in the study area. MMWL is the Mediterranean meteoric water line (Gat and Carmi, 1970), GMWL is the global meteoric water line (Craig, 1961), and LMWL is the local meteoric water line (Bajjali, 2012).

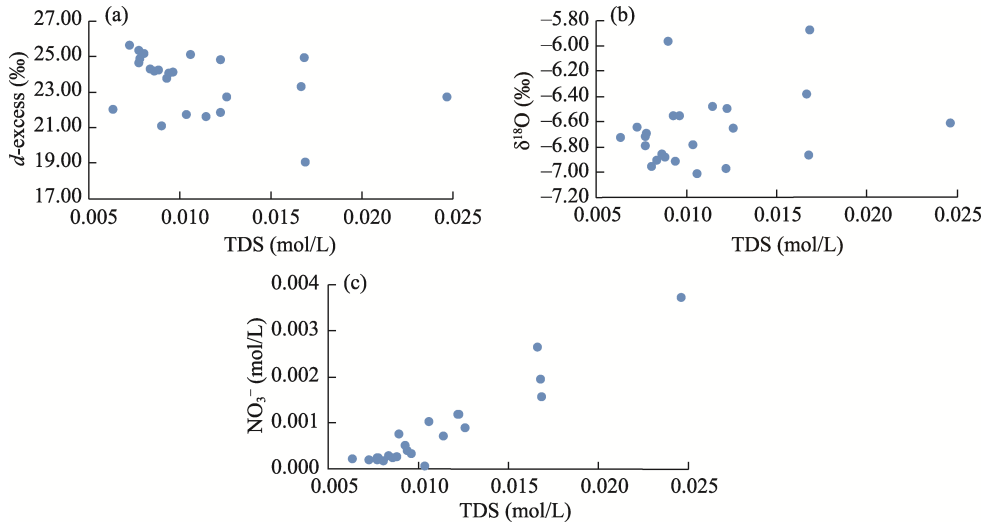

Fig. 8 Relationships of TDS with *d*-excess (a), $\delta^{18}O$ (b), and NO_3^- (c)

have distinct ^{15}N and ^{18}O compositions (Kendall, 1998; Silva et al., 2000). The $\delta^{15}N\text{-}NO_3^-$ values of the different nitrate sources are as follows: nitrate produced by the nitrification of manure or sewage (7.0‰–20.0‰), atmospheric nitrate (–13.0‰–13.0‰), nitrate in synthetic fertilizer (–3.0‰–3.0‰), and natural soil organic matter (3.0‰–5.0‰) (Mayer et al., 2002; Lee et al., 2008; Xue et al., 2009; Gutiérrez et al., 2018; Obeidat et al., 2021b). According to Durka et al. (1994), Mayer et al. (2002), Kendall et al. (2007), and Xue et al. (2009), $\delta^{18}O\text{-}NO_3^-$ values of the different sources are as follows: nitrification-derived nitrate (–15.0‰–15.0‰), atmospheric nitrate (25.0‰–70.0‰), and nitrate in synthetic fertilizer (17.0‰–25.0‰). Fractionation caused by biological, chemical, and physical processes (nitrification, denitrification, assimilation, and volatilization) ultimately leads to the modification of stable isotopic composition of dissolved nitrate (Kaown et al., 2009).

In the study area, $\delta^{15}N\text{-}NO_3^-$ values ranged from 2.6‰ to 13.7‰, with an average of 7.0‰, and$\delta^{18}O\text{-}NO_3^-$ values ranged from 1.1‰ to 7.4‰, with an average of 3.0‰ (Table 5). We can see from Figure 9 that nine samples fall into the category of "manure or septic waste". These samples showed that $\delta^{15}N\text{-}NO_3^-$ and $\delta^{18}O\text{-}NO_3^-$ values are in the ranges of 8.2‰–13.7‰ and 1.5‰–7.4‰, respectively. These results match the values resulting from nitrification of wastewater or manure. The NO_3^- concentrations of these samples varied from 12.4 to 230.8 mg/L, exceeding the natural background NO_3^- concentrations (5.0–10.0 mg/L). Thus, domestic wastewater can be considered the source of pollution in these samples. In addition, nine samples belonged to the overlapping window of "Soil NH_4^+" and "manure or septic waste". $\delta^{15}N\text{-}NO_3^-$ values of these samples varied from 3.7‰ to 7.4‰ and$\delta^{18}O\text{-}NO_3^-$ values ranged from 1.1‰ to 5.5‰. Except that the NO_3^- concentration of the sample from a groundwater well was 3.5 mg/L, which is within the range of natural background value, the NO_3^- concentration of other samples ranged from 13.8 to 54.3 mg/L, which exceeded the natural background value. The stable isotope composition of dissolved nitrate of the sample from a groundwater well suggests soil NH_4^+ as the source of nitrate, whereas other samples contain nitrate from domestic wastewater. The remaining five samples fall into the overlapping window of "manure or septic waste", "soil NH_4^+", and "NH_4^+ in fertilizers and precipitation". $\delta^{15}N\text{-}NO_3^-$ values of these samples varied from 2.6‰ to 4.3‰ and $\delta^{18}O\text{-}NO_3^-$ values ranged from 1.6‰ to 4.3‰. There was a significant positive correlation between Cl^- and $\delta^{15}N$ (r=0.74; P<0.01), indicating domestic waste is the primary source of nitrate.

4.5 Biogeochemical processes

Nitrification is the process of NH_4^+ transformation to nitrate catalysed by many autotrophic bacteria or archaea (Kendall, 1998). Denitrification, on the other hand, is the process by which

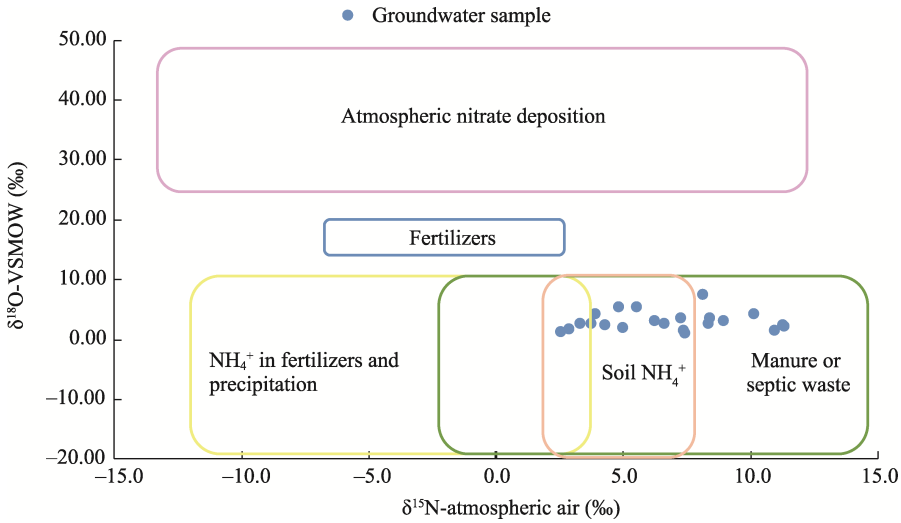

Fig. 9 Plot of δ^{15}N-atmospheric air vs. δ^{18}O-VSMOW of the groundwater samples in the study area. VSMOW is Vienna Standard Mean Ocean Water. The rectangles represent the stable isotopic composition of dissolved nitrate from different sources. The boxes represent the fields of ranges of stable isotopic values of different sources.

nitrates are converted to gaseous phases such as nitrogen, nitrogen dioxide, and nitric oxide under reducing conditions (Brandes and Devol, 1997; Koba et al., 1997). ^{14}N is preferentially deposited in the generated NO_3^- during nitrification if the NH_4^+ substrate is not limited. δ^{18}O-NO_3^- values resulting from nitrification varied from –5‰ to 15‰; these values depended on those of δ^{18}O-H_2O and oxygen gas (Durka et al., 1994; Mayer et al., 2001). δ^{18}O-NO_3^- values in groundwater in the study area varied from 1.1‰ to 7.4‰, with an average of 3.0‰, which is significantly lower than the values of nitrate in fertilizers (17.0‰–25.0‰) and atmospheric nitrate (25.0‰–70.0‰). This indicates that nitrification is the main biochemical process affecting nitrogen species, and wastewater and soil NH_4^+ are the main sources of nitrate. δ^{18}O-H_2O values varies between –25.0‰ and 4.0‰, and the δ^{18}O values of atmosphere is approximately 23.5‰. δ^{18}O-NO_3^- values generated by nitrification fluctuate in the range of –10.0‰ to 10.0‰ (Kendall et al., 2007). We estimated the theoretical δ^{18}O-NO_3^- generated by bacterial nitrification using δ^{18}O values measured for groundwater in the study area and assuming that the δ^{18}O of ambient oxygen gas is 23.5‰. Accordingly, the calculated theoretical δ^{18}O-NO_3^- values in groundwater ranged from 2.4‰ to 3.1‰, with an average of 2.6‰, which are within the measured δ^{18}O-NO_3^- values (1.1‰–7.4‰). In general, the average measured δ^{18}O-NO_3^- value (3.0‰) was consistent with the average calculated theoretical δ^{18}O-NO_3^- value for nitrification. Denitrification takes place under the following circumstances (Gutierrez et al., 2018): low concentrations of DO (1.0–2.0 mg/L), availability of electron donors, denitrifying bacteria, trace nutrients, nitrate, temperature (25°C–35°C), and pH (5.5–8.0). The abovementioned circumstances are not found in the study area, where the DO concentrations are higher than 4.0 mg/L, and groundwater temperature does not exceed 25°C.

5 Conclusions and recommendations

The integrated hydrochemical methods, environmental isotope techniques, and multivariate statistical analysis have been successfully applied to explore the provenance, quality, and pollution of groundwater in the Amman-Al Zarqa Basin, Jordan. The invasion of domestic wastewater into fresh groundwater has caused the deterioration of water quality and its evolution from Ca-Mg-HCO_3 to Ca-Mg-Cl and Ca-Mg-SO_4. The groundwater of the study area comes from rainfall in the Mediterranean Sea and is a part of the current water cycle, as proven by its stable isotope composition. Altitude and rainfall amount are the main factors affecting the stable isotope composition of groundwater. The main source of pollution is domestic wastewater, as indicated by

the stable isotope composition of dissolved nitrate. Moreover, nitrification is the main biochemical process governing nitrogen species. Water–rock interaction (dissolution and cation exchange) is the main natural process affecting groundwater quality. The results of this study provide an important tool for decision-makers to implement effective groundwater protection measures. It is highly recommended to apply best management practices and efficient land use planning, including improved agriculture (e.g., fertilization, manure application, and storage of animal manures) and sanitation techniques (e.g., better design of pit latrines and septic tanks as well as sewer leakage control).

Conflict of interest

The authors declare that they have no known competing financial interests or personal relationships that could have appeared to influence the work reported in this paper.

Acknowledgements

This study was funded by the Deanship of Scientific Research, Jordan University of Science and Technology (20210159).

Author contributions

Conceptualization: Mutawakil OBEIDAT, Ahmad AL-AJLOUNI; Data curation: Mutawakil OBEIDAT; Methodology: Mutawakil OBEIDAT; Investigation: Muna ABU-DALO; Formal analysis: Mutawakil OBEIDAT; Writing - original draft preparation: Eman BANI-KHALED; Writing - review and editing: Eman BANI-KHALED, Muheeb AWAWDEH, Muna ABU-DALO; Funding acquisition: Mutawakil OBEIDAT, Ahmad AL-AJLOUNI; Resources: Muheeb AWAWDEH, Muna ABU-DALO; Supervision: Mutawakil OBEIDAT, Ahmad AL-AJLOUNI; Project administration: Mutawakil OBEIDAT, Ahmad AL-AJLOUNI; Software: Muheeb AWAWDEH, Eman BANI-KHALED; Validation: Mutawakil OBEIDAT; Visualization: Muna ABU-DALO.

References

Abascal E, Gómez-Coma L, Ortiz I, et al. 2022. Global diagnosis of nitrate pollution in groundwater and review of removal technologies. Science of The Total Environment, 810: 152233, doi: 10.1016/j.scitotenv.2021.15223.

Abu-Alnaeem M F, Yusoff I, Ng T F, et al. 2018. Assessment of groundwater salinity and quality in Gaza coastal aquifer, Gaza Strip, Palestine: An integrated statistical, geostatistical and hydrogeochemical approaches study. Science of The Total Environment, 615: 972–989.

Adimalla N, Qian H, Nandan M J. 2020. Groundwater chemistry integrating the pollution index of groundwater and evaluation of potential human health risk: A case study from hard rock terrain of south India. Ecotoxicology and Environmental Safety, 206: 111217, doi: 10.1016/j.ecoenv.2020.111217.

Aeschbach-Hertig W, El-Gamal H, Dahab K, et al. 2007. Identifying and dating the origin of groundwater resources in reclamation areas of Egypt. In: Advances in Isotope Hydrology and its Role in Sustainable Water Resources Management. Vienna, Austria.

Afroza R, Mazumder Q H, Jahan C S, et al. 2009. Hydrochemistry and origin of salinity in groundwater in parts of lower Tista floodplain, Northwest Bangladesh. Journal of the Geological Society of India, 74(2): 223–232.

Alam S M, Li P, Fida M. 2023. Groundwater nitrate pollution due to excessive use of N-fertilizers in rural areas of Bangladesh: pollution status, health risk, source contribution, and future impacts. Exposure and Health, doi: 10.1007/s12403-023-00545-0.

Al-Alawneh M. 1998. Hydrology and hydrochemistry of Wadi Jerash catchment area. MSc Thesis. Baghdad: University of Baghdad.

Al-Fugara A k, Ahmadlou M, Al-Shabeeb A R, et al. 2022. Spatial mapping of groundwater springs potentiality using grid search-based and genetic algorithm-based support vector regression. Geocarto International, 37(1): 284–303.

Al-Kharabsheh A. 2020. Challenges to sustainable water management in Jordan. Jordan Journal of Earth and Environmental Sciences, 11(1): 38–48.

Al Mahamid J. 2005. Integration of water resources of the upper aquifer in Amman-Zarqa basin based on mathematical

modeling and GIS, Jordan. Freiberg Online Geology, doi: 10.23689/fidgeo-879.

Al Wreikat M A, Al-Kharabsheh A A. 2020. Impact of over-pumping on groundwater resources sustainability at Amman Zarqa basin, Jordan: A case study of arid areas affected by Syrian refugees crisis. Environmental Earth Sciences, 79(1): 1–8.

APHA (American Public Health Association). 1998. Standard Methods for the Examination of Water and Wastewater (20th ed.). Washington DC: American Public Health Association, American Water Works Association, and Water Environmental Federation.

Appelo C A J, Postma D. 2005. Geochemistry, Groundwater and Pollution (2nd ed.). London: A.A. Balkema Publishers.

Aravinthasamy P, Karunanidhi D, Subramani T, et al. 2020. Fluoride contamination in groundwater of the Shanmuganadhi River basin (south India) and its association with other chemical constituents using geographical information system and multivariate statistics. Geochemistry, 80(4): 125555, doi: 10.1016/j.chemer.2019.125555.

Ayadi Y, Mokadem N, Besser H, et al. 2018. Statistical and geochemical assessment of groundwater quality in Teboursouk area (Northwestern Tunisian Atlas). Environmental Earth Sciences, 77(9): 1–20.

Bajjali W. 2012. Spatial variability of environmental isotope and chemical content of precipitation in Jordan and evidence of slight change in climate. Applied Water Science, 2(4): 271–283.

Barzegar R, Asghari Moghaddam A, Tziritis E. 2017. Hydrogeochemical features of groundwater resources in Tabriz plain, northwest of Iran. Applied Water Science, 7(7): 3997–4011.

Bender F. 1974. Geology of Jordan. Berlin: Gebrueder Borntraeger.

Brandes J A, Devol A H. 1997. Isotopic fractionation of oxygen and nitrogen in coastal marine sediments. Geochimica et Cosmochimica Acta, 61(9): 1793–1801.

Buzeta R K. 2019. Nitrate contaminant tracing in surface and groundwater in the Great Miami River Watershed: Environmental isotope approach. PhD Dissertation. Dayton: University of Dayton.

Carrey R, Ballesté E, Blanch A R, et al. 2021. Combining multi-isotopic and molecular source tracking methods to identify nitrate pollution sources in surface and groundwater. Water Research, 188: 116537, doi: 10.1016/j.watres.2020.116537.

Chadha D. 1999. A proposed new diagram for geochemical classification of natural waters and interpretation of chemical data. Hydrogeology Journal, 7(5): 431–439.

Craig H. 1961. Isotopic variations in meteoric waters. Science, 133(3465): 1702–1703.

Dansgaard W. 1964. Stable isotopes in precipitation. Tellus, 16(4): 436–468.

Das S, Nag S. 2017. Application of multivariate statistical analysis concepts for assessment of hydrogeochemistry of groundwater—a study in Suri I and II blocks of Birbhum District, West Bengal, India. Applied Water Science, 7(2): 873–888.

Durka W, Schulze E D, Gebauer G, et al. 1994. Effects of forest decline on uptake and leaching of deposited nitrate determined from ^{15}N and ^{18}O measurements. Nature, 372(6508): 765–767.

Dutton A, Wilkinson B H, Welker J M, et al. 2005. Spatial distribution and seasonal variation in $^{18}O/^{16}O$ of modern precipitation and river water across the conterminous USA. Hydrological Processes: An International Journal, 19(20): 4121–4146.

El Yaouti F, El Mandour A, Khattach D, et al. 2009. Salinization processes in the unconfined aquifer of Bou-Areg (NE Morocco): A geostatistical, geochemical, and tomographic study. Applied Geochemistry, 24(1): 16–31.

Elmeknassi M, Bouchaou L, El Mandour A, et al. 2022. Multiple stable isotopes and geochemical approaches to elucidate groundwater salinity and contamination in the critical coastal zone: A case from the Bou-areg and Gareb aquifers (North-Eastern Morocco). Environmental Pollution, 300: 118942, doi: 10.1016/j.envpol.2022.118942.

Gat J, Carmi I. 1970. Evolution of the isotopic composition of atmospheric waters in the Mediterranean Sea area. Journal of Geophysical Research, 75(15): 3039–3048.

Gibbs R J. 1970. Mechanisms controlling world water chemistry. Science, 170(3962): 1088–1090.

Gibrilla A, Fianko J R, Ganyaglo S, et al. 2020. Nitrate contamination and source apportionment in surface and groundwater in Ghana using dual isotopes (^{15}N and ^{18}O-NO_3) and a Bayesian isotope mixing model. Journal of Contaminant Hydrology, 233: 103658, doi: 10.1016/j.jconhyd.2020.103658.

Gutiérrez M, Biagioni R N, Alarcón-Herrera M T, et al. 2018. An overview of nitrate sources and operating processes in arid and semiarid aquifer systems. Science of The Total Environment, 624: 1513–1522.

Hammouri N, El-Naqa A. 2007. Hydrological modeling of ungauged wadis in arid environments using GIS: A case study of Wadi Madoneh in Jordan. Revista Mexicana de Ciencias Geológicas, 24(2): 185–196.

Hammouri N, El-Naqa A. 2008. GIS based hydrogeological vulnerability mapping of groundwater resources in Jerash area-Jordan. Geofísica Internacional, 47(2): 85–97.

He S, Li P, Su F, et al. 2022. Identification and apportionment of shallow groundwater nitrate pollution in Weining Plain,

northwest China, using hydrochemical indices, nitrate stable isotopes, and the new Bayesian stable isotope mixing model (MixSIAR). Environmental Pollution, 298: 118852, doi: 10.1016/j.envpol.2022.118852.

Hem J D. 1985. Study and Interpretation of the Chemical Characteristics of Natural Water (3rd ed.). Charlottesville: University of Virginia.

Jalali M. 2009. Geochemistry characterization of groundwater in an agricultural area of Razan, Hamadan, Iran. Environmental Geology, 56(7): 1479–1488.

Jasechko S, Perrone D, Befus K M, et al. 2016. Global aquifers dominated by fossil groundwaters but wells vulnerable to modern contamination. Nature Geoscience, 10: 425–429.

Jia H, Howard K, Qian H. 2020. Use of multiple isotopic and chemical tracers to identify sources of nitrate in shallow groundwaters along the northern slope of the Qinling Mountains, China. Applied Geochemistry, 113: 104512, doi: 10.1016/j.apgeochem.2019.104512.

Jordan Standards and Metrology Organization. 2015. Water–Drinking Water, Technical Regulation. [2023-01-27]. https://www.unhcr.org/jo/wp-ontent/uploads/sites/60/2019/08/Annex-A-1-Technical-Regulation-of-Jordan-Standards-and-Metrology-Organization.pdf.

Jung H, Koh D-C, Kim Y S, et al. 2020. Stable isotopes of water and nitrate for the identification of groundwater flowpaths: A review. Water, 12(1): 138, doi: 10.3390/w12010138.

Kaown D, Koh D-C, Mayer B, et al. 2009. Identification of nitrate and sulfate sources in groundwater using dual stable isotope approaches for an agricultural area with different land use (Chuncheon, mid-eastern Korea). Agriculture, Ecosystems & Environment, 132(3–4): 223–231.

Kattan Z. 2019. Factors controlling stable isotopes variability in precipitation in Syria: Statistical analysis approach. Journal of Earth System Science, 128(6): 1–25.

Kendall C. 1998. Tracing Nitrogen Sources and Cycling in Catchments. Amsterdam: Elsevier.

Kendall C, Elliott E M, Wankel S D. 2007. Tracing anthropogenic inputs of nitrogen to ecosystems. In: Michener R, Lajtha K. Stable Isotopes in Ecology and Environmental Science (2nd ed.). doi: 10.1002/9780470691854.ch12.

Koba K, Tokuchi N, Wada E, et al. 1997. Intermittent denitrification: the application of a ^{15}N natural abundance method to a forested ecosystem. Geochimica et Cosmochimica Acta, 61(23): 5043–5050.

Kou X, Ding J, Li Y, et al. 2021. Tracing nitrate sources in the groundwater of an intensive agricultural region. Agricultural Water Management, 250: 106826, doi: 10.1016/j.agwat.2021.106826.

Lee K S, Bong Y S, Lee D, et al. 2008. Tracing the sources of nitrate in the Han River watershed in Korea, using $\delta^{15}N\text{-}NO_3^-$ and $\delta^{18}O\text{-}NO_3^-$ values. Science of The Total Environment, 395(2–3): 117–124.

Li P, Qian H. 2018. Water resouorces research to support as sustinable China. International Journal of Water Resources Development, 34(3): 327–336.

Li P, Wang D, Li W, et al. 2022. Sustainable water resources development and management in large river basins: An introduction. Environmental Earth Sciences, 81: 179, doi: 10.1007/s12665-022-10298-9.

Linhoff B. 2022. Deciphering natural and anthropogenic nitrate and recharge sources in arid region groundwater. Science of The Total Environment, 848: 157345, doi: 10.1016/j.scitotenv.2022.157345.

Liu J, Gao Z, Feng J, et al. 2023. Identification of the hydrochemical features, genisis, water quality and potential health hazards of groundwater in Dawen River Basin, North China. Ecological Indicators, 149: 110175, doi: 10.1016/j.ecolind.2023.110175.

Machiwal D, Cloutier V, Güler C, et al. 2018. A review of GIS-integrated statistical techniques for groundwater quality evaluation and protection. Environmental Earth Sciences, 77(19): 1–30.

Marandi A, Shand P. 2018. Groundwater chemistry and Gibbs diagram. Applied Geochemistry, 97: 209–212.

Mayer B, Bollwerk S M, Mansfeldt T, et al. 2001. The oxygen isotope composition of nitrate generated by nitrification in acid forest floors. Geochimica et Cosmochimica Acta, 65(16): 2743–2756.

Mayer B, Boyer E W, Goodale C, et al. 2002. Sources of nitrate in rivers draining sixteen watersheds in the northeastern US: Isotopic constraints. Biogeochemistry, 57(1): 171–197.

Mcilvin M R, Altabet M A. 2005. Chemical conversion of nitrate and nitrite to nitrous oxide for nitrogen and oxygen isotopic analysis in freshwater and seawater. Analytical Chemistry, 77(17): 5589–5595.

Meybeck M. 1987. Global chemical weathering of surficial rocks estimated from river dissolved loads. American Journal of Science, 287(5): 401–428.

MWI (Ministry of Water and Irrigation). 2023. National Water Strategy 2023–2040: Summary. Jordan: Ministry of Water and

Irrigation.

Obeidat M M, Massadeh A M, Al-Ajlouni A M, et al. 2007. Analysis and evaluation of nitrate levels in groundwater at Al-Hashimiya area, Jordan. Environmental Monitoring and Assessment, 135: 475–486.

Obeidat M, Awawdeh M, Abu Al-Rub F, et al. 2012. An innovative nitrate pollution index and multivariate statistical investigations of groundwater chemical quality of Umm Rijam Aquifer (B4), North Yarmouk River Basin, Jordan. In: Voudouris V. Water Quality Monitoring and Assessment. Croatia: InTech.

Obeidat M, Awawdeh M, Abu Al-Rub F. 2013. Multivariate statistical analysis and environmental isotopes of Amman/Wadi Sir (B2/A7) groundwater, Yarmouk river Basin, Jordan. Hydrological Processes, 27(17): 2449–2461.

Obeidat M, Awawdeh M, Matiatos I, et al. 2021a. Identification and apportionment of nitrate sources in the phreatic aquifers in Northern Jordan using a dual isotope method ($\delta^{15}N$ and $\delta^{18}O$ of NO_3^-). Groundwater for Sustainable Development, 12: 100505, doi: 10.1016/j.gsd.2020.100505.

Obeidat M, Awawdeh M, Al-Kharabsheh N, et al. 2021b. Source identification of nitrate in the upper aquifer system of the Wadi Shueib catchment area in Jordan based on stable isotope composition. Journal of Arid Land, 13(4): 350–374.

Panno S, Kelly W, Martinsek A, et al. 2006. Estimating background and threshold nitrate concentrations using probability graphs. Groundwater, 44(5): 697–709.

Popescu R, Mimmo T, Dinca O R, et al. 2015. Using stable isotopes in tracing contaminant sources in an industrial area: A case study on the hydrological basin of the Olt River, Romania. Science of The Total Environment, 533: 17–23.

Prasanna M V, Chidambaram S, Srinivasamoorthy K. 2010. Statistical analysis of the hydrogeochemical evolution of groundwater in hard and sedimentary aquifers system of Gadilam river basin, South India. Journal of King Saud University-Science, 22(3): 133–145.

Qu S, Duan L, Mao H, et al. 2023. Hydrochemical and isotopic fingerprints of groundwater origin and evolution in the Urangulan River Basin, China's Loess Plateau. Science of The Total Environment, 866: 161377, doi: 10.1016/j.scitotenv.2022.161377.

Reddy A G S, Niranjan Kumar K, Subba Rao D, et al. 2009. Assessment of nitrate contamination due to groundwater pollution in north eastern part of Anantapur District, A.P. India. Environmental Monitoring and Assessment, 148(1): 463–476.

Ren X, Li P, He X, et al. 2021. Hydrogeochemical processes affecting groundwater chemistry in the central part of the Guanzhong Basin, China. Archives of Environmental Contamination and Toxicology, 80(1): 74–91.

Rezaei A, Hassani H, Tziritis E, et al. 2020. Hydrochemical characterization and evaluation of groundwater quality in Dalgan basin, SE Iran. Groundwater for Sustainable Development, 10: 100353, doi: 10.1016/j.gsd.2020.100353.

Rimawi O. 1985. Hydrochemistry and isotope hydrology of groundwater and surface water in the north-east of Mafraq, Dhuleil, Hallabat, Azraq basin. PhD Dissertation. Munich: Technical University of Munich.

Rozanski K, Araguás-Araguás L, Gonfiantini R. 1993. Isotopic patterns in modern global precipitation. Geophysical Monograph-American Geophysical Union, 78, doi: 10.1029/GM078p0001.

Sajil Kumar P, James E. 2016. Identification of hydrogeochemical processes in the Coimbatore district, Tamil Nadu, India. Hydrological Sciences Journal, 61(4): 719–731.

Salameh E, Alraggad M, Tarawneh A. 2014. Natural salinity sources in the groundwaters of Jordan–importance of sustainable aquifer management. Geochemistry, 74(4): 735–747.

Salameh E, Bannayan H. 1993. Water Resources of Jordan. Future and Future Potentials. Amman: Friedrich Ebert Stiftung.

Salman A, Al-Qinna M, Al-Kuisi M. 2014. Spatial analysis of soil and shallow groundwater physiochemical parameters in El-Mujib Basin-central Jordan. Journal of Asian Earth Sciences, 79: 366–381.

Samtio M S, Hakro A A A, Jahangier T M, et al. 2023. Impact of rock-water interaction on hydrogeochemical characteristcs of groundwater: using multivariate statistical, water quality idex and irrigation indices of chachro sub-district, thar desert, sindh, Pakistan. Groundwater for Sustainable Development, 20: 1008878, doi: 10.1016/j.gsd.2022.100878.

Schoeller H. 1977. Geochemistry of Groundwater. Groundwater Studies, An International Guide for Research and Practice. Paris: UNESCO.

Selvam S, Venkatramanan S, Chung S. 2016. Identification of groundwater contamination sources in Dindugal district of Tamil Nadu, India using GIS and multivariate statistical analyses. Arabian Journal of Geosciences, 9(5): 1–14.

Silva S, Kendall C, Wilkison D, et al. 2000. A new method for collection of nitrate from fresh water and the analysis of nitrogen and oxygen isotope ratios. Journal of Hydrology, 228(1–2): 22–36.

Su F, Wu J, Wang D, et al. 2022. Moisture movement, soil salt migration, and nitrogen transformation under different irrigation conditions: field experimental research. Chemosphere, 300: 134569, doi: 10.1016/j.chemosphere.2022.134569.

Tarawneh M S M, Janardhana M, Ahmed M M. 2019. Hydrochemical processes and groundwater quality assessment in North eastern region of Jordan valley, Jordan. HydroResearch, 2: 129–145.

Tiwari A K, Pisciotta A, De Maio M. 2019. Evaluation of groundwater salinization and pollution level on Favignana Island, Italy. Environmental Pollution, 249: 969–981.

Todd D K. 1980. Groundwater Hydrology. New York: Wiley.

Torres-Martínez J A, Mora A, Knappett P S, et al. 2020. Tracking nitrate and sulfate sources in groundwater of an urbanized valley using a multi-tracer approach combined with a Bayesian isotope mixing model. Water Research, 182: 115962, doi: 10.1016/j.watres.2020.115962.

Toumi N, Hussein B H, Rafrafi S. 2015. Groundwater quality and hydrochemical properties of Al-Ula region, Saudi Arabia. Environmental Monitoring and Assessment, 187(3): 1–16.

UN (United Nations). 2019. The Sustainable Development Goals Report. New York: United Nations.

Venkatesan S, Arumugam S, Bagyaraj M, et al. 2021. Spatial assessment of groundwater quantity and quality: A case study in parts of Chidambaram Taluk, Cuddalore District, Tamil Nadu, India. Sustainable Water Resources Management, 7(6): 1–17.

Wang S, Zheng W, Currell M, et al. 2017. Relationship between land-use and sources and fate of nitrate in groundwater in a typical recharge area of the North China Plain. Science of The Total Environment, 609: 607–620.

Weyhenmeyer G A, Hartmann J, Hessen D O, et al. 2019. Widespread diminishing anthropogenic effects on calcium in freshwaters. Scientific Reports, 9: 10450, doi: 10.1038/s41598-019-46838-w.

WHO (World Health Organization). 2011. Guidelines for drinking-water quality. WHO Chronicle, 38(4): 104–108.

Wu J, Li P, Qian H, et al. 2014. Using correlation and multivariate statistical analysis to identify hydrogeochemical processes affecting the major ion chemistry of waters: A case study in Laoheba phosphorite mine in Sichuan, China. Arabian Journal of Geosciences, 7: 3973–3982.

Xue D, Botte J, De Baets B, et al. 2009. Present limitations and future prospects of stable isotope methods for nitrate source identification in surface-and groundwater. Water Research, 43(5): 1159–1170.

Yang H, Xiao Y, Hao Q, et al. 2023. Geochemical characteristics, mechanisms and suitability for sustainable municipal and agricultural water supply of confined groundwater in central North China plain. Urban Climate, 49: 101459, doi: 10.1016/j.uclim.2023.101459.

Zaidi F K, Nazzal Y, Jafri M K, et al. 2015. Reverse ion exchange as a major process controlling the groundwater chemistry in an arid environment: A case study from northwestern Saudi Arabia. Environmental Monitoring and Assessment, 187(10): 1–18.

Zhang Q, Shu W, Li F, et al. 2022. Nitrate source apportionment and risk assessment: A study in the largest ion-adsorption rare earth mine in China. Environmental Pollution, 302: 119052, doi: 10.1016/j.envpol.2022.119052.

Zhang Y, Zhang Q, Chen W, et al. 2023. Hydrochemical analysis and groundwater pollution source identification based on self-organizing map at a contaminated site. Journal of Hydrology, 616: 128839, doi: 10.1016/j.jhydrol.2022.128839.

Zhu A, Chen J, Gao L, et al. 2019. Combined microbial and isotopic signature approach to identify nitrate sources and transformation processes in groundwater. Chemosphere, 228: 721–734.